Applied Surface Science Advances 5 (2021) 100123

Contents lists available at ScienceDirect

Applied Surface Science Advances

journal homepage: www.sciencedirect.com/journal/applied-surface-science-advances

# TEOS thin films obtained by plasma polymerization on $Ti_6Al_4V$ alloys: Influence of the deposition pressure on surface properties and cellular response

Mireli Pereira [a], Estela Kerstner Baldin [a,*], Leonardo Marasca Antonini [a], Fabiano Bernardi [b], Luiza Oliveira [c], Natasha Maurmann [c], Patricia Pranke [c,d], Marcelo Barbalho Pereira [e], Célia de Fraga Malfatti [a]

[a] LAPEC/PPGE3M, Federal University of Rio Grande do Sul (UFRGS), Av. Bento Gonçalves, 9500, 91501-970, Porto Alegre, RS, Brazil
[b] Graduate Program in Physics, Institute of Physics, Federal University of Rio Grande do Sul (UFRGS), Av. Bento Gonçalves, 9500, Porto Alegre, RS, Brazil
[c] Hematology and Stem Cell Laboratory, Faculty of Pharmacy Federal University of Rio Grande do Sul (UFRGS), Avenida Ipiranga, 2752, 90610-000, Porto Alegre, RS, Brazil
[d] Stem Cell Research Institute (IPCT), Avenida Ipiranga, 2752, 90610-000, Porto Alegre, RS, Brazil
[e] Laser and Optics Laboratory, Federal University of Rio Grande do Sul (UFRGS), Av. Bento Gonçalves, 9500, 91501-970, Porto Alegre, RS, Brazil

ARTICLE INFO

*Keywords:*
Thin films
TEOS
Plasma polymerization
Stem cells

ABSTRACT

The modification of surfaces by the application of thin films has been used in the regenerative medicine area to increase the biocompatibility of metal implants. Titanium alloy has been recently used as substrate in polymerization for biomedical application. In this context, silane films were obtained by plasma polymerization in favor of the sol-gel method and the influence of different pressures in obtaining these films by argon plasma polymerization was evaluated from the alkoxysilane precursor tetraethoxysilane (TEOS) on the $Ti_6Al_4V$ alloy. The morphological characterization of the films was performed by AFM, Profilometry and Spectral Ellipsometry and the chemical composition was analyzed by XPS. The biological behavior was evaluated by analyzing the mitochondrial activity and cellular viability of mesenchymal stem cells. The plasma polymerization process resulted in the deposition of a nanometric Si-based film formed, predominantly, by Si-O and organosilane bonds. The films that were applied on a sanded surface, with lower pressures in the plasma polymerization process, presented a lower layer thickness and wettability than the films obtained on nanotextured surfaces. Considering absorbance values, the $Ti_6Al_4V$ samples mechanically sanded and deposited by plasma polymerization at 230 μatm presented better cell viability than samples with nanotextured surfaces coated with plasma polymerized film, indicating this material has potential to biomedical application.

## Introduction

Silane films are commonly obtained by the sol-gel method. However, due to the improvement in the deposition techniques, alternative methods with emphasis on plasma polymerization have been developed [1,2]. In this case, according to Batan et al. [1], plasma acts on the chemical decomposition of the silane precursor, generating a source of active species, which, when deposited on the surface, promotes the formation of a film with similar composition to the precursor itself.

Plasma polymerization has some advantages over the sol-gel method. For example, it has less steps and its operational parameters may be adjusted, thus allowing the control of properties such as thickness and chemical composition. In addition, according to Batan et al. [1], the plasma technique made it possible to obtain a higher degree of crosslinking of the siloxane network (Si−*O*−Si) than the sol-gel method, when depositing a film based on organoalkoxysilane precursor on aluminum substrates.

In biomaterials, Finke et al. [3] found that the application of nanometric films polymerized by plasma, using the precursors allylamine (PPAAm) and ethylenediamine (PPEDA) on titanium substrates, provided surface changes that favored the growth of osteoblastic cells, enabling the use of these films for application in bioengineering. In vitro

* Corresponding author.
*E-mail address:* estelakerstner@gmail.com (E.K. Baldin).

https://doi.org/10.1016/j.apsadv.2021.100123
Received 16 March 2021; Received in revised form 1 June 2021; Accepted 9 June 2021
Available online 19 June 2021

studies, developed by Rebl et al. [4], Nebe et al. [5] and Testrich et al. [6], also demonstrated that polymerized films on titanium and $Ti_6Al_4V$ alloy surfaces showed greater adhesion of MG-63 cells than on uncoated substrates. In addition, Gabler et al. [7] found that titanium implants with the deposition of films obtained by precursors based on amine had a positive effect on the adhesion of bone cells and consequently on the osseointegration process in vivo. For the application in regenerative medicine, some authors have observed the possibility of controlling the operational parameters using plasma to obtain polymeric films, which provides surface properties that improved the interaction between stem cells by inducing osteogenic differentiation with more ease [8,9,10,11].

As shown by Chou et al. [12] parylene (or poly-para-xylene) coating is considered an effective barrier. It is a possible alternative to the conventional parylene coating for use in surface modification of biomedical devices. Li et al. [13] showed an improvement in the corrosion resistance of biomedical nickel titanium (NiTi) when a polymeric allylamine film is deposited by plasma polymerization. The polymeric film increased the polarization resistance. Thus, corrosion resistance is also improved, and the plasma-polymerized coating may reduce corrosion risks of biomedical NiTi alloy in clinical use. Zhou et al. [14] showed that a hexamethyldisiloxane film deposited on Ti6Al4V improve its corrosion resistance in hanks solution. The siloxane film used to coat Ti6Al4V samples is more compact and cross-linked and,. consequently, it has better corrosion resistance. Li et al. [15] have also improved the corrosion resistance and hemocompatibility of biomedical NiTi alloy when (2,2,3,4,4,4-Hexafluorobutyl methacrylate) polymer coating was deposited by plasma polymerization in the presence of a fluorine-containing precursor.

Few publications are focused on investigating the characterization and evaluation of different parameters for obtaining silane films by plasma polymerization. In view of the innovative character and the advantages presented by it, the importance of developing these is emphasized materials for application in the area of tissue engineering. Thus, this work aimed at investigating the influence of different pressures in obtaining thin films based on the silane precursor tetraethoxysilane (TEOS) by plasma polymerization on sanded and nanotextured $Ti_6Al_4V$ alloys, evaluating surface, electrochemical properties and biological behavior through the use of mesenchymal stem cells.

## Experimental section

### *Surface treatment*

Grade 5 $Ti_6Al_4V$ samples were obtained from a polycrystalline cylindrical bar of 14 mm in diameter and 1 m long, with a thickness of 2 mm. The mechanical sanding of these samples occurred gradually using SiC sandpaper from #180 to 5000. After sanding, the samples were cleaned in an ultrasonic bath with acetone, ethyl alcohol and deionized water for 5 min. Finally, the samples were dried in air flow.

After characterizing the samples, in order to evaluate the influence of nanotexturing on the deposition of silane films obtained by the plasma process, the samples were subjected to an electrolytic polishing process. For this, the samples of $Ti_6Al_4V$, with an area of approximately 1.5 $cm^2$, were electropolished in an acid solution composed of sulfuric acid, hydrofluoric acid and glycerin in the proportion 6:3:1 (v/v), using an energy source (MPC-303DI, Minipa, São Paulo, Brazil) with platinum as the cathode (area of approximately 2.0 $cm^2$). Electropolishing was carried out at 25 V at a temperature of 7 ± 0.5 °C for 4 min. and after all samples were washed in deionized water using an ultrasonic bath for 10 min and dried with cold air.

The polymerization process was carried out using the silane precursor Tetraethoxysilane - $Si(OC_2H_5)_4$, TEOS, subjected to different pressures: 230, 300, 400 and 500 μatm, for 20 min at room temperature (≈ 23 °C). Argon was used as carrier gas with purity of 99.999%.

The plasma film deposition was performed in an apparatus built at the Corrosion Research Laboratory (LAPEC/UFRGS). The samples were placed inside a glass container and fixed in an adapted titanium support, in order to facilitate the passage of plasma through the entire surface. Inside this container, a vacuum of around 500 μatm of pressure was achieved, monitored by an electronic vacuometer CPS VG100A and using a 12 cfm double stage dual voltage vacuum pump.

Subsequently, an inert atmosphere was created by the injection of argon gas, which acted as carrier gas, once in contact with the silane precursor. Then, an electrical discharge of the radiofrequency (RF) type was applied to promote the generation of plasma and consequently the formation of a polymerized film on the metallic substrate.

## Characterization

The XPS measurements were performed in an Omicron Sphera analyzer using an Al K-α X-ray source ($h\nu = 1486.7$ eV). The x-ray source was positioned at 80° in relation to the emission beam direction of the photoelectrons. The samples were attached to the holder without further preparation and inserted in the ultrahigh vacuum chamber ($\sim 5 \times 10^{-9}$ mbar). The measurements were performed in the Long Scan, Si 2p, O 1 s and C 1 s electronic regions of the samples. A pass energy of 50 eV and 10 eV was used, as well as an energy step of 1 eV and 0.1 eV and 0.1 s dwell time for the Long Scan and high resolution XPS regions, respectively. The calibration of the electron analyzer was performed using an Au standard and considering the Au $4f_{7/2}$ peak position at 84.0 eV. Furthermore, the adventitious C was considered at 284.5 eV in the C 1 s region to verify possible charging effects.

The Si 2p XPS spectra were analyzed with the XPSPeak 4.1 software using a Shirley-type background and a symmetric Gaussian-Lorentzian sum function with 18% Lorentzian contribution, as determined from the analysis of the Au 4f XPS region of the Au standard used. The binding energy and FWHM values of a given chemical component were constrained to the same value for all samples.

The nanometric surface roughness of the samples as well as the topographic profile was measured in an atomic force microscope SPM-9500J3 SHIMADZU operating in contact mode, with silicon nitride probes (Nanosensors) and scanner with vertical variation of 4 μm and scanning area of 2 μm x 2 μm. The evaluation of the surface roughness through the AFM was carried out through the measures of Ra (arithmetic mean of the absolute values of the spacing ordinates of the points of the roughness profile in relation to the midline, within the measurement path) and Rz (arithmetic mean of the five partial roughness values, considering the greatest distance points, above and below the midline).

The micrometric roughness of the samples was determined by using a MITUTOYO SJ-400 profilometer, obtaining the values of Ra (μm) and Rz (μm) from 0.8 mm cut offs [16]. All measurements were performed in triplicate. According to the information provided by the manufacturer of the profilometer, the Ra parameter defines the arithmetic mean of absolute values over the entire length of the sample, while the Rz is based on the five highest peaks and lowest valleys along the entire length.

The thickness of the obtained films was determined by spectral ellipsometry (Sopra GES-5E). This technique measures the change in the state of light polarization after it reflects in the sample at an angle of 75°, wavelength range of 0.3500 to 0.7500 μm (steps of 0.005 μm) and correlates this change to a physical model of the film, in order to obtain the dispersion curve of the film and its physical thickness.

The contact angle measurements, used to determine the surface wettability, were performed using the sessile drop method, with equipment developed by the Corrosion Research Laboratory (LAPEC) at the Federal University of Rio Grande do Sul (Porto Alegre, Brazil), in which a drop of liquid was deposited on the surface using a micropipette. The drop was observed through low magnification lenses and the contact angle was measured with a goniometer. Contact angle measurements were performed with water and a simulated body fluid solution (Hank's solution) [17].

## Biological tests

The mesenchymal stem cells (MSC) used in this work are known as SHED (Stem Cells from Human Exfoliated Deciduous teeth) and the cultures were established according to previous studies [18,19].

In a laminar flow hood, the pulp of the teeth was digested with collagenase and the cells were cultured at 37 °C and 5% $CO_2$ in low glucose DMEM medium supplemented with 10% Bovine Fetal Serum (SFB) and 1% antibiotic (penicillin and streptomycin). Whenever confluence was reached, the culture was cultured using 0.05% Trypsin/EDTA. The dissociated cells were then transferred at a density of 5000 cells per $cm^2$. Thus, subsequent passages were performed, and cell cultures were evaluated on the fourth pass.

Prior to carrying out the experiments, the cells were characterized as human mesenchymal stem cells according to the recommendations of the International Society for Cellular Therapy (ISCT) [20].

Stem cells were characterized as follows: (1) cell morphological evaluation and ability to adhere to plastic; (2) immunophenotypic analysis of cells by means of flow cytometry and (3) the ability to differentiate osteogenic, adipogenic and chondrogenic in vitro [21,22,19].

First, the samples were sterilized for 1 hour in UV. The stem cells (30,000 per well) were seeded in the tissue culture plate (TCP, used as a control) and in the samples. After 1 day of cultivation, the viability of the cells was assessed using the MTT mitochondrial activity assay ([Bromide of [3-(4,5-dimethylthiazole-2yl)−2,5-diphenyl tetrazolium]). MTT was used at a concentration of 0.25 $mg.mL^{-1}$ in CMF buffer for an incubation time of 3 h at 37 °C [21,22]. After that time, the supernatants from the wells were discarded and the formazan crystals formed were dissolved with 500 μL of dimethyl sulfoxide (DMSO) and 300 μL read in a Multiskan™ FC (Thermo Scientific - Thermo Fisher Scientific®) spectrophotometer. The results were calculated by the absorbance difference at 630 and 570 nm wavelengths.

The samples were washed in phosphate buffer, fixed in 4% paraformaldehyde buffer and the cell nuclei were stained with 0.5 $\mu g.mL^{-1}$ of 4,6-diamidino-2-phenylindole (DAPI) in accordance with the protocol proposed by Maurmann and collaborators [21]. Photographs were obtained with a fluorescence microscope (Leica Dmi8, Leica Microsystems).

Cell viability was also visualized by fluorescein diacetate (FDA) and propidium iodide (IP) staining in a LIVE/DEAD type assay. The supernatants from the culture wells were discarded and washed with phosphate buffer. Then 10 $\mu g.mL^{-1}$ of FDA and 5 $\mu g.mL^{-1}$ of IP dissolved in phosphate buffer were added, and the images were obtained by fluorescence microscopy (Leica Dmi8, Leica Microsystems).

The results were expressed as the mean ± standard error of the mean and evaluated using one-way ANOVA (no significant differences were established). An independent *t*-test was used to compare the groups ($*p < 0.05$ and $**p < 0.01$). Data analyses were performed with the program BioEstat 5.0.

## Results and discussion

Fig. 1 shows the Long Scan (a) and Si 2p XPS spectra (b) of the samples following the nomenclature presented in Table 1. The Long Scan spectra show the presence of Ti, V, Al, Si, N, C, and O in all samples. The presence of V, Ti and Al comes from the substrate and C and O atoms comes from the exposition of the samples to the atmosphere, besides the products formed during synthesis of the silicone-based thin films. The small amount of N is probably remnant from the synthesis procedure adopted. Moreover, the $Ti_6Al_4V$/PP230 sample presents Ca atoms that come as residues adsorbed at the surface from the water used before the polymerization process.

The analysis of the Si 2p XPS spectra shows the presence of a chemical component at 101.8 eV in all samples, which is associated to organo-oxysilane [23]. Additionally, those samples synthesized with smaller pressures (230 and 300 μatm) present the Si-O component at 103.0 eV associated to Si-O bonds ($Si_xO_y$) [24]. Some authors [25,26] reported the formation of thin films of lower surface energy for smaller polymerization pressures, then increasing the cross-link and improving the mechanical properties of the coating synthesized.

Based on the XPS results, two mechanisms for the formation of films

**Table 1**
Sample nomenclature.

| | |
|---|---|
| $Ti_6Al_4V$ | $Ti_6Al_4V$ mechanically sanded substrate up to #5000. |
| $Ti_6Al_4V_{nano}$ | $Ti_6Al_4V$ mechanically sanded substrate to #5000 and nanostructured. |
| $Ti_6Al_4V$/PP230 | $Ti_6Al_4V$ mechanically sanded substrate to #5000, with deposition of silane film by plasma polymerization at 230 μatm. |
| $Ti_6Al_4V_{nano}$/PP230 | $Ti_6Al_4V$ mechanically sanded substrate to #5000, nanotextured, with deposition of silane film by plasma polymerization at 230 μatm. |
| $Ti_6Al_4V$/PP300 | $Ti_6Al_4V$ mechanically sanded substrate to #5000, with silane film deposition by plasma polymerization at 300 μatm. |
| $Ti_6Al_4V$/PP400 | $Ti_6Al_4V$ mechanically sanded substrate to #5000, with silane film deposition by plasma polymerization at 400 μatm. |
| $Ti_6Al_4V$/PP500 | $Ti_6Al_4V$ mechanically sanded substrate to #5000, with the deposition of silane film by plasma polymerization at 500 μatm. |

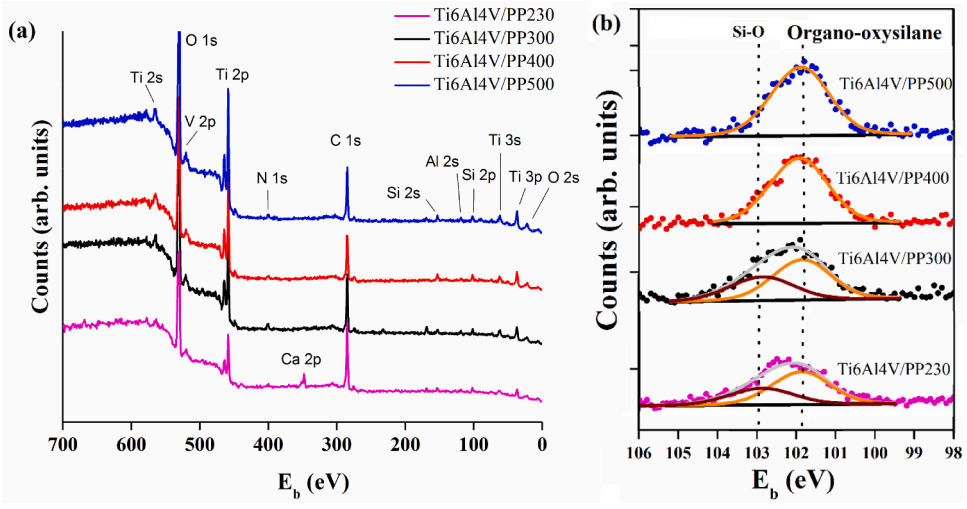


**Fig. 1.** XPS spectra at the (a) Long Scan and (b) Si 2p regions of the samples polymerized by argon plasma and the corresponding fit (gray line) at the Si 2p region (pink line $Ti_6Al_4V$/PP230, black line $Ti_6Al_4V$/PP300, red line $Ti_6Al_4V$/PP400 and blue line $Ti_6Al_4V$/PP500). .

were proposed: the first is based on a final product with the formation of the Si−O bond, related to the Si−O−Si siloxane bond (Fig. 2) and the second proposing the formation of the Si−C bond, organo-oxysilane (Fig. 3).

Through the reactions shown in Fig. 2, two TEOS molecules react. In one of them, the O−$CH_2$ bond breaks and in the other the Si−O bond breaks. After the rupture of these connections, reactive centers are generated with the $^{\bullet}OSi\text{-}R_3$; group approaching the $^{\bullet}O\text{-}CH_2\text{—}CH_3$ to the $^{\bullet}CH_2\text{—}CH_3$ group. The formation of the final product of the reaction occurs through the formation of the Si-O-Si (siloxane) bond, associated with the $CH_3\text{—}CH_2\text{—}O\text{-}CH_2\text{—}CH_3$ by-product, both also proposed by Franquet [25], Kim et al. [26], Han et al. [27] and Sharan et al. [28].

The second mechanism also occurs by the reaction of two TEOS molecules. In one of them, the O—$CH_2$ bond is broken and in the other the Si-O bond is broken After the disruption of these connections and the formation of reactive centers, $^{\bullet}CH_2\text{—}CH_3$ group is brought to the $^{\bullet}Si\text{-}R_3$ group and, at the same time, the $^{\bullet}O\text{-}CH_2\text{—}CH_3$ group to the $^{\bullet}OSi\text{-}R_3$. The formation of the final product with the Si-C bond is described in Fig. 3.

Based on the XPS results, the second reaction mechanism prevailed in the films obtained in this study, that is, the peak intensity of the Si-C bond was higher than the Si-O. For the deposition of the alkoxide film, the alkyl fragments originating from TEOS are adsorbed on the substrate and cross-formation occurs, generating Si-O-Si. According to Lee et al. [29], the presence of argon in the polymerization process increases the ionization degree and decreases the oxidation process of the precursors used, due to the increased electron impact mechanism. For Kim [30], excited oxygen atoms (íons $O_2^{+}$) lead to the formation of Si-O-Si bonds and consequently favor film growth. For Chung et al. [31] and Teshima et al. [32] during the polymerization process, in addition to the formation of Si-O-Si bonds, the formation of $SiO_2$ can occurs through the oxidation of Si atoms.

In this study, due to the thickness of the films, their morphology could not be analyzed by SEM. It was necessary to use the AFM technique, as indicated by Schaefer et al. [33]. Fig. 4 shows the images obtained by atomic force microscopy for the determination of the nanometric topographic profiles of the evaluated systems, in which for the sanded-only sample, the presence of grooves from the mechanical preparation used was evidenced. For the sample obtained from plasma polymerization at 230 μatm, the presence of a greater number of granular deposits was uniformly distributed over the analyzed surface. According to Bazaka et al. [34] during the plasma deposition, certain regions of the coating become more susceptible to the arrangement of surface bonds and changes in the rate with which the material is being deposited on the surface. Certain morphologies favor the accumulation of polymer on the peaks and ridges, while others promote deposition of the polymer within the gaps and voids on the surface. At micro, nano and sub-nano scales, the surface of the substratum may affect the deposition of the reactive species and thus the chemical and biological activity of the coating.

When plasma comes into contact with sanded samples, the polymer species begin to assemble on the peaks of the nanoscale features on the surface and a surface load may build up. This can lead to the formation of a strong dipole-like electric field pattern, which increases the flow of ions from the plasma bulk towards the surface. The distribution of ions results in the deposition of plasma-derived building blocks between the already formed polymer islands, resulting in the gradual filling of the gaps and voids on the surface. The strong electric field that is formed at the nanoscale surface promotes the formation of a smooth coating via nucleation of a newly deposited phase between the surface features and already nucleated islands [35,36].

With the increase in polymerization pressure, from 300 μatm to 500 μatm, the deposit regions have decreased, and have been evenly distributed in the direction of the grooves from the mechanical preparation. Such result can be related to a higher deposition rate observed for the film obtained under less pressure, since according to the formation of the layer of this type of film, it occurs from a self-organized nucleation process [7].

Along with this, the greater pressure difference between the reaction chamber and the silane precursor reservoir may have provided greater energy. Consequently, a greater number of nucleation points were formed, as well as the layer and, consequently, the surface irregularity (higher nanometric and micrometric Rz values) also increased.

The values of the nanometric and micrometric roughness parameters (Ra and Rz) were consistent with the topographic profiles previously observed, in which for all sanded samples polymerized at pressures greater than 230 μatm, and lower and similar values were observed for the average nanometric and micrometric (Ra). However, in relation to the Rz values in both the nanometric scale and the micrometric scale, higher values were obtained for the polymerized sample at the lowest pressure (230 μatm). This increase in Rz roughness may be associated

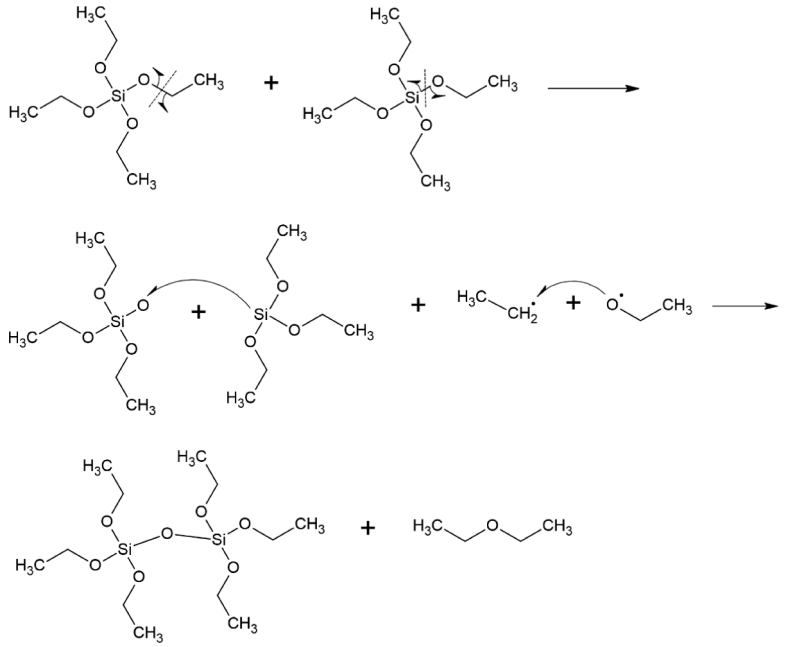

**Fig. 2.** First proposed mechanism for the formation of a final product with Si−O−Si bond.

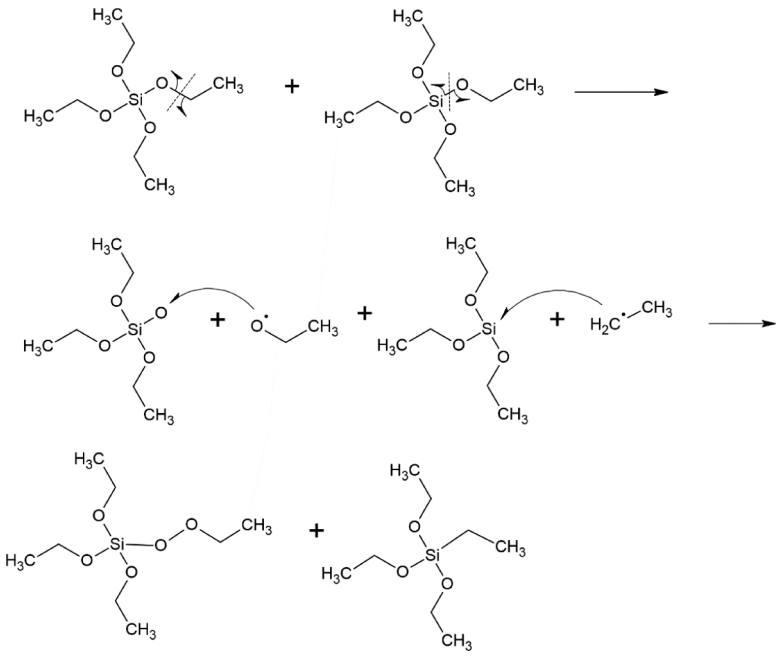

**Fig. 3.** Second proposed mechanism for the formation of a final product with Si-C bond.

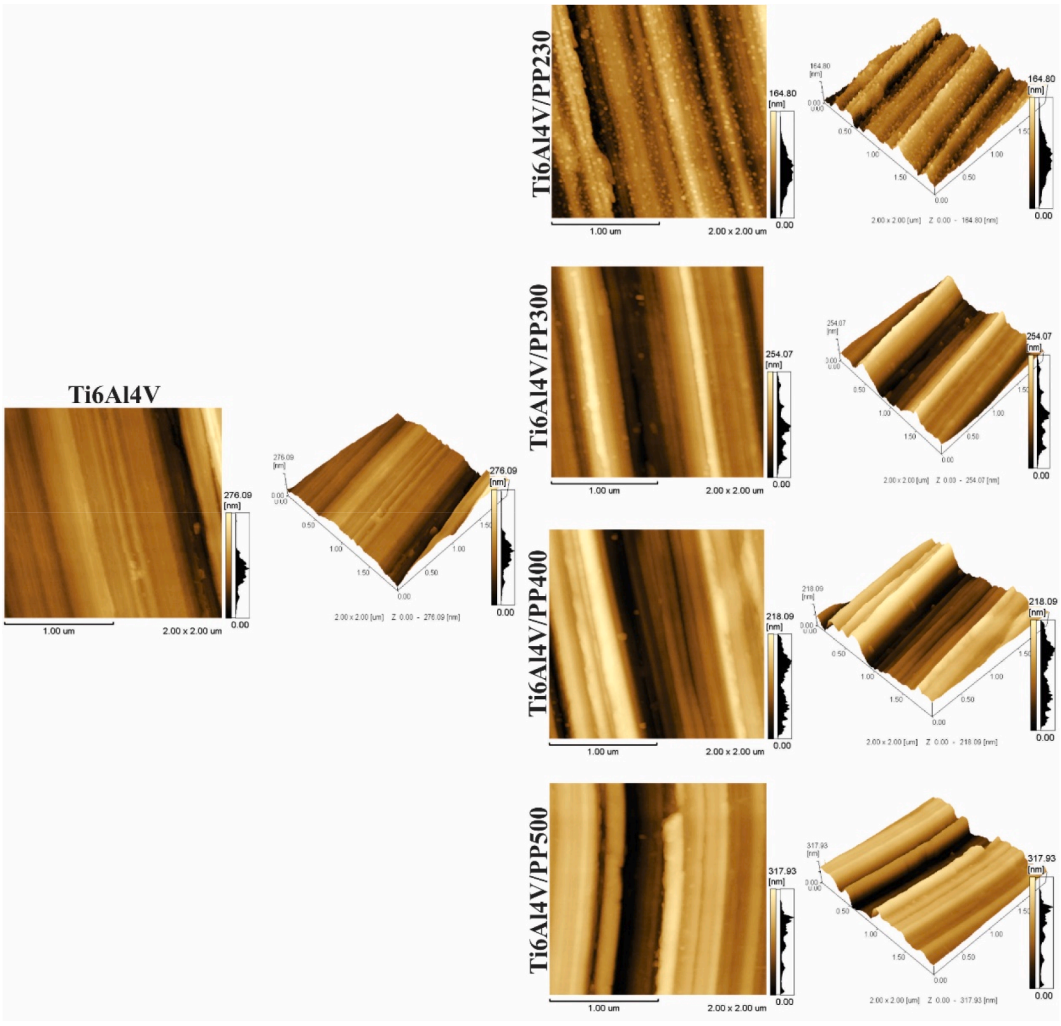


**Fig. 4.** AFM images of silane films obtained by plasma polymerization at different pressures.

with the use of a low polymerization pressure, which favored an increase in deposition in the higher regions of the topographic profile, consequently resulting in an increase in Rz roughness.

The contact angle measurements indicated lower values for the $Ti_6Al_4V$/PP230 system, which was polymerized at a lower pressure, indicating a greater surface wettability than the sanded and plasma-polymerized systems. Such observation may be associated with the greater Rz roughness or greater deposition of the TEOS films in this pressure. The influence of pressure on the deposition rate of the films can also be evidenced by the fact that normally the surface wettability varies according to the roughness parameters [1].

Table 3 presents the results of the layer thicknesses of the films obtained at different pressures. Corroborating with the previously discussed results, the greater thickness presented by the sample $Ti_6Al_4V$/PP230, can again be associated with the ability that the process of plasma polymerization performed at lower pressures has to act predominantly by the mechanism of dissociation by impact of electrons. The amount of ionized fragments formed has increased and, as a consequence, the polymerization and binding of the molecules with the metallic substrate have also increased.

The effect of the electrochemical nanotexturization surface treatment was evaluated on the $Ti_6Al_4V$/PP230 sample, as this film showed a more uniform deposition over the entire surface of the metallic substrate, with a higher layer thickness deposited than the other evaluated systems.

Fig. 5

Table 2

Table 4

Fig. 6(a) presentes the XPS spectra at the Long Scan and Fig. 6(b) the Si2p regions of the nanostructured surface of $Ti_6Al_4V_{nano}$/PP230. The results presented in Fig. 6(a) show the presence of elements such as Ti and O related to the titanium oxide formed on the surface sample. Furthermore, in Fig. 6(a) the presence of the elements O and Si is verified and in Fig. 6(b) the Si-O and Si-C bonds are associated with the Si-based film deposited by plasma polymerization.

Fig. 7 shows the nanometric surface topographies of the electropolished Ti6Al4V surface only and with the deposition of the polymerized silane film. Regarding the roughness parameters, it was possible to observe higher micrometric Rz values for the $Ti_6Al_4V_{nano}$/PP230 sample compared to the nanotextured sample ($Ti_6Al_4V_{nano}$). Such behavior can be related to the sum of processes involved, since there is a greater irregularity of the nanotextured surface due to the competition between the anodic dissolution and the thickening of the oxide layer during the performance of this electrochemical treatment. Combined with the subsequent deposition of the polymerized film, the deposition in higher regions of the surface may have been favored, resulting in higher Rz values on a micrometric scale.

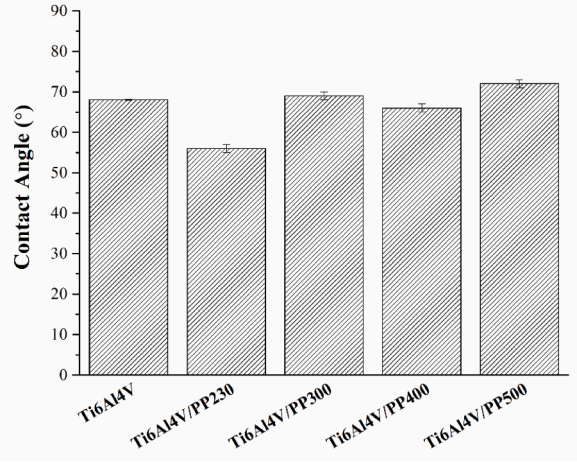


**Fig. 5.** Contact angle measurements in Hank's solution.

**Table 2**
Nanometric and micrometric roughness measurements determined by AFM and contact profilometry.

| Sample | AFM | | Profilometry | |
|---|---|---|---|---|
| | Ra (nm) | Rz (nm) | Ra (μm) | Rz (μm) |
| $Ti_6Al_4V$ | 9 ± 2 | 15 ± 3 | 0.10 ± 0.01 | 1.00 ± 0.10 |
| $Ti_6Al_4V$/PP230 | 4 ± 2 | 33 ± 8 | 0.10 ± 0.02 | 1.20 ± 0.10 |
| $Ti_6Al_4V$/PP300 | 4 ± 1 | 15 ± 2 | 0.10 ± 0.01 | 0.30 ± 0.04 |
| $Ti_6Al_4V$/PP400 | 5 ± 1 | 12 ± 2 | 0.10 ± 0.01 | 0.30 ± 0.01 |
| $Ti_6Al_4V$/PP500 | 5 ± 1 | 9 ± 2 | 0.10 ± 0.01 | 0.40 ± 0.10 |

**Table 3**
Thickness of films obtained by plasma polymerization determined by ellipsometry.

| Sample | Thickness (nm) |
|---|---|
| $Ti_6Al_4V$/PP230 | 10.00 ± 0.30 |
| $Ti_6Al_4V$/PP300 | 3.82 ± 0.40 |
| $Ti_6Al_4V$/PP400 | 2.53 ± 0.27 |
| $Ti_6Al_4V$/PP500 | 1.39 ± 0.24 |

**Table 4**
Nanometric and micrometric roughness measurements.

| Sample | Nanometric roughness (AFM) | | Micrometric roughness (Profilometry) | |
|---|---|---|---|---|
| | Ra (nm) | Rz (nm) | Ra (μm) | Rz (μm) |
| $Ti_6Al_4V_{nano}$ | 14 ± 3 | 37 ± 8 | 0.20 ± 0.01 | 1.50 ± 0.20 |
| $Ti_6Al_4V_{nano}$/PP230 | 9 ± 2 | 34 ± 10 | 0.30 ± 0.03 | 2.50 ± 0.10 |

The contact angle measurements (Fig. 8) show a decrease in the contact angle values of the nanotextured sample polymerized by plasma ($Ti_6A1_4V_{nano}$). In other words, the wettability increased in Hank's solution. A greater wettability may be associated with deposition by plasma polymerization of the TEOS film, since the structure of the precursor promotes a polar character to the film, which leads to a greater interaction with water and aqueous fluids. As reported by Attarilar et al. [37] the contact angle reduction (greater wettability) and the large number of pores are the preferred regions for cell proliferation and adhesion.

The thickness measurements of the films showed that $Ti_6Al_4V$/PP230, which was only sanded and polymerized by plasma had a thickness of ~ 10 nm, while the sample nanotextured with plasma ($Ti_6Al_4V_{nano}$/PP230) obtained a thickness of ~ 18 nm. These results indicate a significant contribution of the nanotexturization to the deposition by plasma polymerization. The only nanotextured sample ($Ti_6Al_4V_{nano}$) had a thickness of 5.0 ± 0.2 nm, which could be associated to the $TiO_2$ layer formed during the electrochemical treatment. Such oxide has been reported by Antonini et al. [38].

*Biological behavior*

In the mitochondrial activity assay (Fig. 9), ANOVA analysis of variance detected no statistical difference among the experimental groups ($p = 0.0858$). The MTT results shown in Fig. 9 and the images of the stained cell nuclei, as well as the live and dead stem cells (Fig. 10) showed a similarity in the number of cells in the different samples. According to Ortiz et al. [39], stem cells have a greater affinity for anchoring in grooves from sanded surfaces. Bao et al. [40] and Attarilar et al. [41] stated that a superficial topography with micrometric and textured roughness tends to promote a greater growth of stem cells due to the presence of cell adhesion sites. Furthermore, Wang et al. [42] showed that modern topographies associated with the wettability may facilitate the fast osseointegration and adhesion of cells.

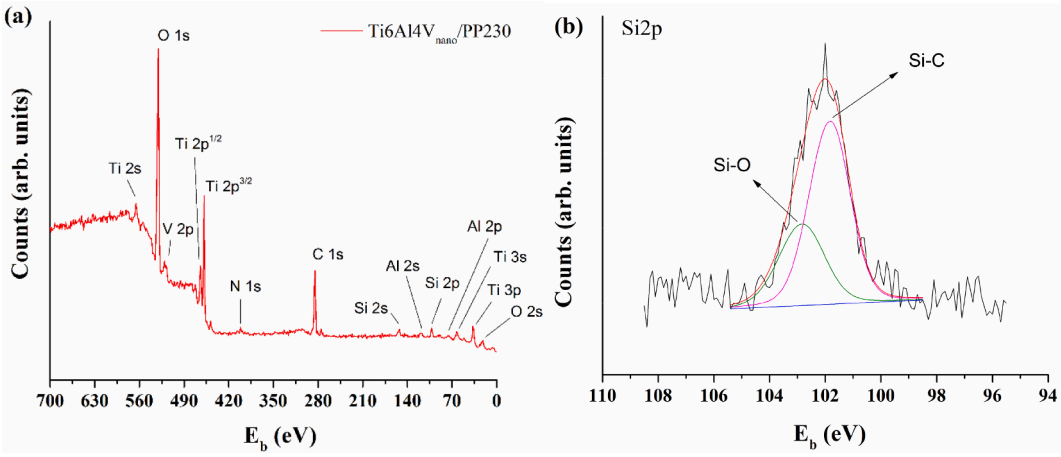


**Fig. 6.** XPS spectra at the Long Scan (a) and Si 2p (b) regions of the nanostructured surface of $Ti_6Al_4V_{nano}$/PP230 sample and the corresponding fit (gray line) at the Si 2p region.

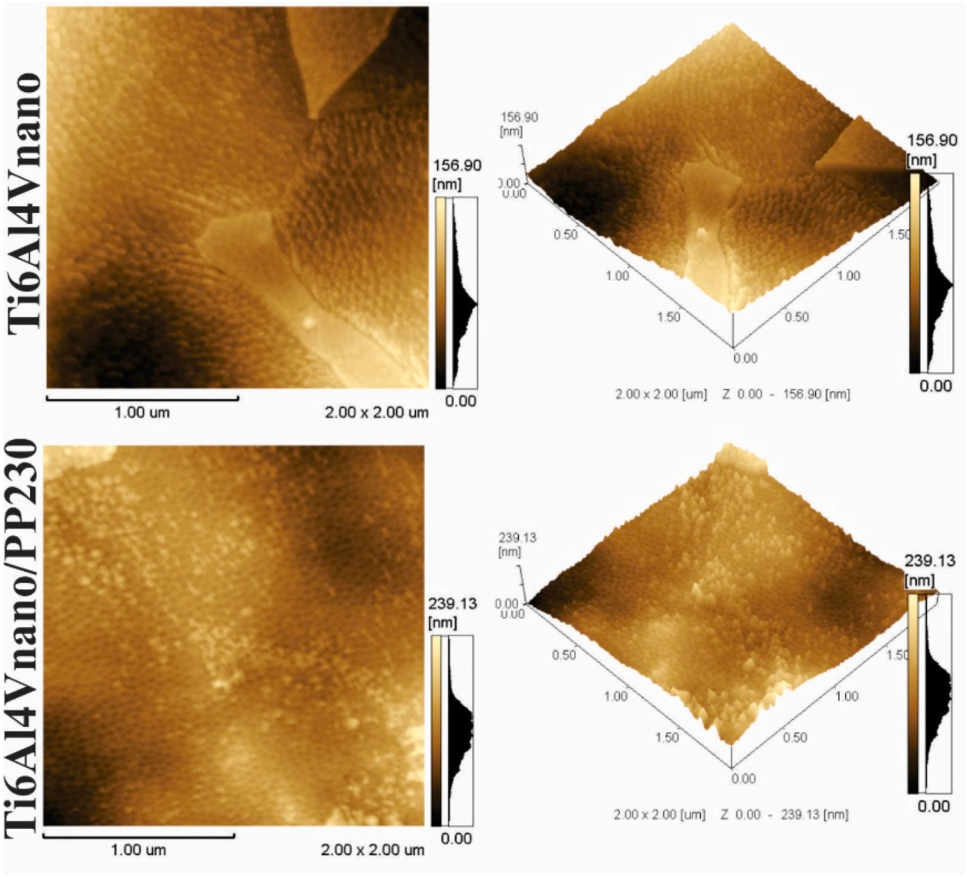


**Fig. 7.** Two-dimensional and three-dimensional AFM images of the sample with nanotextured and nanotextured surfaces with plasma polymerization.

In the present study, it was possible to observe only a trend towards a greater amount of SHED in the sanded Ti6Al4V samples.

On the other hand, the evaluation with the *t*-test comparing the $Ti_6Al_4V$ samples and the samples that were polymerized by plasma to argon, demonstrated a greater number of viable stem cells than the polymerized nanotextured surface, with ps of 0.0399 and 0.0044, respectively. As shown by S. Hwang et al. [43], films polymerized by air plasma, in addition to being nanometric in thickness, tend to follow the topography of the metallic substrate. The results of the present study indicate that the irregularities of the mechanical sanding present in the sanded samples remained below the plasma polymerized film. These surfaces probably favored the anchoring of stem cells on the surfaces, since both experimental groups have similar absorbance correlated to the number of viable SHEDs ($p = 0.2783$). This study was carried out using the TEOS film to improve the surface properties of Ti6Al4V. However, as observed in the results, the film did not add significant improvements compared to the sanded sample. In addition, analyzing Fig. 9, it is evident that there was no statistical difference between the sanded sample ($Ti_6Al_4V$) and the sanded sample with polymerized film ($Ti_6Al_4V$/PP230).

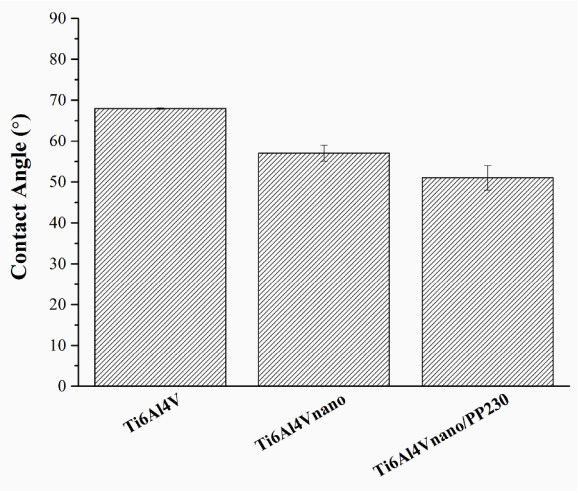


**Fig. 8.** Contact angle measurements in Hank's solution.

In addition, a certain orientation was observed for the $Ti_6Al_4V$ and $Ti_6Al_4V$/PP230 samples, as shown in Fig. 10, probably induced by the topography from the mechanical preparation. On the nanotextured surfaces ($Ti_6Al_4V_{nano}$ and $Ti_6Al_4V_{nano}$/PP230) the stem cells showed a disoriented disposition during cell culture, similar to the culture plate used as a control. According to Rebl et al. [44] the rough surfaces positively influence osteoblast behavior, that increasing roughness results in a cell attachment. The cells and their actin cytoskeleton are oriented in the direction of the grooves. Lüthen et al. [45] showed that the highest level of rat osteoblast cell attachment was obtained with rougher surface. Some authors [46,47] have shown that osteoblast cells cultured on materials with grooves become elongated parallel to the direction of the grooves.

## Conclusions

Nanometric Si films were obtained through the argon plasma polymerization process on the $Ti_6Al_4V$ substrate, based on two formation mechanisms, where Si−O and organo-oxysilane (Si−C) bonds were predominant.

The use of different pressures resulted in a greater layer thickness for

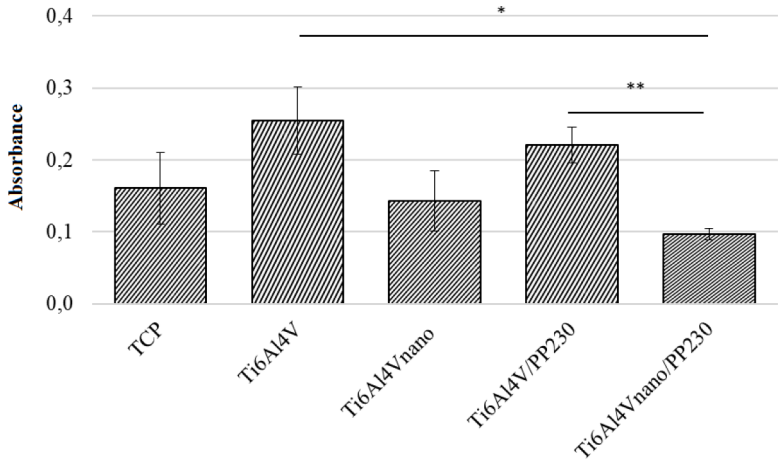


**Fig. 9.** Viability of mesenchymal stem cells cultured on films obtained by plasma polymerization. Data expressed as mean absorbance ± standard error of the mean using the MTT test. $*p < 0.05$ and $**p < 0.001$. Data are given from $n = 3$ (n represents number of samples tested for each system).

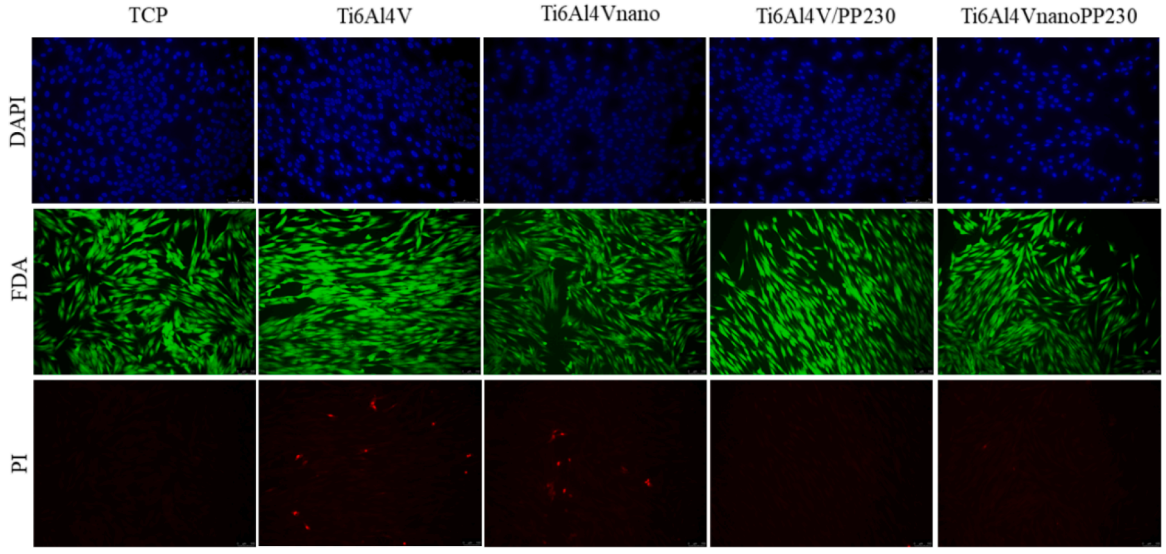


**Fig. 10.** Fluorescence microscopy with representative images of cell nuclei marked in blue (stained with DAPI), viable cells in green (stained with FDA) and non-viable in red (stained with PI) in the different experimental groups after 24 h of culture.

the polymerized film at a lower pressure on the sanded sample., No difference among the chemical composition of the films obtained could be found. However, the film deposited on the nanostructures showed a greater surface roughness and, in addition, provided an increase in wettability and in layer thickness in relation to the nanostructured substrate. This increase has probably taken place due to the presence of oxygen in the film composition, favoring the formation of hydrogen bonds with water. The films that were applied on a sanded surface, with lower pressures in the plasma polymerization process, presented a lower layer thickness and wettability than the films obtained on nanotextured surfaces.

The biological results showed that the only sanded surface tended to have a greater number of viable mesenchymal stem cells, due to their ability to anchor in the grooves from mechanical preparation. The samples sanded and polymerized by plasma showed a higher number of viable stem cells than the nanotextured and polymerized surface by plasma. The irregularities resulting from mechanical sanding associated with the thin film obtained by plasma polymerization may have contributed to the maintenance of cell viability due to the anchoring of stem cells. Samples with nanotextured surfaces with plasma-polymerized films did not favor the viability of stem cells, with lower absorbance results than the mechanically sanded groups and deposition of silane film by plasma polymerization at 230 μatm ($Ti_6Al_4V$). The $Ti_6Al_4V$ samples favored cell viability, when compared to the lower absorbance values obtained with samples with nanotextured surfaces with plasma polymerized film.

## Declaration of Competing Interest

The authors declare that they have no known competing financial interests or personal relationships that could have appeared to influence the work reported in this paper.

## Acknowledgments

The present work was carried out with the support of Brazilian Government entities focused on human resources formation, with support of National Council of Technological and Scientific Development (CNPq, Process 155466/2018–6) and Coordination for the Improvement of Higher Education Personnel (CAPES – PROEX Process 23038.000341/2019–71). Ministry of Science, Technology, Innovation and Communication (MCTIC). Furthermore, Célia de Fraga Malfatti acknowledges CNPq (Grant 307723/2018-6), Fabiano Bernardi acknowledges CNPq (Grant 312526/2018–0) and Marcelo Barbalho Pereira acknowledges CNPq (Grant 407542/2018–3) and Research Support Foundation of the State of Rio Grande do ul, FAPERGS (Grant 20/2551–0000276–4). The authors thank LAMAS-UFRGS staff for the assistance on the XPS measurements.

## References

[1] A. Batan, F. Brusciotti, I. De Graeve, J. Vereecken, M. Wenkin, M. Piens, J. J. Pireaux, F. Reniers, H. Terryn, Comparison between wet deposition and plasma deposition of silane coatings on aluminium, Prog. Org. Coat. 69 (2010) 126–132, v.
[2] T. Xue, S. Attarilar, S. Liu, X. Song, L. Li, B. Zhao, Y. Tang, Surface modification techniques of titanium and its alloys to functionally optimize their biomedical properties: thematic review, Front. Bioeng. Biotechnol. 8 (1–19) (2020) v.
[3] B. Finke, F. Hempel, H. Testrich, A. Artemenko, H. Rebl, O. Kylian, J. Meichsner, H. Biederman, B. Nebe, K.D. Weltmann, Plasma processes for cell-adhesive titanium surfaces based on nitrogen-containing coatings, Surf. Coat. Technol. 205 (2011) S520–S524.
[4] H. Rebl, B. Finke, R. Lange, K.-.D. Weltmann, J.B. Nebe, Impacto f plasma chemistry versus titanium suurface topography on osteoblast orientation, Acta Biomater. 8 (2012) 3840–3851.
[5] B. Nebe, B. Finke, F. Luthen, C. Bergemann, K. Schroder, J. Rychly, K. Liefeith, A. Ohl, Improved initial osteoblast functions on amino-functionalized titanium surfaces, Biomol. Eng. 24 (2007) 447–454.
[6] H. Testrich, H. Rebl, B. Finke, F. Hempel, B. Nebe, J. Meichsner, Aging effects of plasma polymerized ethylenediamine (PPEDA) thin films on cell-adhesive implant coatings, Mater. Sci. Eng. C 33 (2013) 3875–3880, v.
[7] C. Gabler, C. Zietz, R. Gohler, A. Fritsche, T. Lindner, M. Haenle, B. Finke, J. Meichsner, S. Lenz, B. Frerich, F. Luthen, J.B. Nebe, R. Bader, Evaluation of osseointegration of titanium alloyed implants modified by plasma polimerization, Int. J. Mol. Sci. 15 (2014) 2454–2464, v.
[8] M.N. Macgregor-Ramiasa, K. Vasilev, Plasma Polymer Deposition: a Versatile Tool for Stem Cell Research, Adv. Surf. Stem Cell Res. (2016) n.8.
[9] M.K. Markova, E. Radeva, D. Mitev, K. Hristova-Panusheva, B. Paull, P. Nesterenko, J. Sepitka, I. Junkar, A. Iglic, N. Krasteva, Increased elastic modulus of plasma polymer coatings reinforced with detonation nanodiamond particles improves osteogenic differentiation of mesenchymal stem cells, Turk. J. Biol.. v. 42 (2) (2018) 195–203, n.
[10] X. Liu, Q. Feng, A. Bachhuka, K. Vasilev, Surface modification by allylamine plasma polymerization promotes osteogenic differentiation of human adipose-derived stem cells, ACS Appl. Mater. Interfaces 12 (6) (2014) 9733–9741, vn.
[11] S. Zouaghi, T. Six, S. Bellayer, Y. Coffinier, M. Abdallah, N.E. Chihib, C. André, G. Delaplace, M. Jimenez, Atmospheric pressure plasma spraying of silane-based coatings targeting whey protein fouling and bacterial adhesion management, Appl. Surf. Sci. 455 (2018) 392–402, v.
[12] C.M. Chou, K.C. Hsieh, C.J. Chung, J.L. He, Preparation of plasma-polymerized para-hylene as an alternative to parylene coating for biomedical surface modification, Surf. Coat. Technol. 204 (2010) 1631–1636, v.
[13] P. Li, G. Wu, R. Xu, W. Wang, S. Wu, K.W.K. Yeung, P.K. Chu, In vitro corrosion inhibition on biomedical shape memory alloy by plasma-polymerized allylamine film, Mater. Lett. 89 (2012) 51–54, v.
[14] L. Zhou, G.H. Lv, C. Ji, S.Z. Yang, Application of plasma polymerized siloxane films for the corrosion protection of titanium alloy, Thin Solid Films 520 (2012) 2505–2509, v.
[15] P. Li, L. Li, W. Wang, W. Jin, X. Liu, K.W.K. Yeung, P.K. Chu, Enhanced corrosion resistance and hemocompatibility of biomedical NiTi alloy by atmospheric-pressure plasma polymerized fluorine-rich coating, Appl. Surf. Sci. 297 (2014) 109–115, v.
[16] International Organization for Standardization. (1996). Geometrical Product Specifications (GPS) — Surface texture: profile method — Rules and procedures for the assessment of surface texture (ISO 4288:1996). https://www.iso.org/standard/2096.html.
[17] J.H. Hank, Hank's balanced salt solution and pH control, Tissue Cult. Assoc. (1) (1975) 3–4, v.
[18] L. Bernardi, S.B. Luisi, R. Fernandes, T.P. Dalberto, L. Valentim, J.A.B. Chies, A.C. F. Medeiros, P. Pranke, The isolation of stem cells from human deciduous teeth pulp is related to the physiological process of resorption, J. Endod. 37 (2011) 973–979.
[19] F.P. dos Santos, T. Peruch, S.J.V. Katami, A.P.R. Martini, T.A. Crestani, K. Quintiliano, N. Maurmann, E.F. Sanches, C.A. Netto, P. Pranke, A. de Souza Pagnussat, Poly (lactide-co-glycolide) (PLGA) Scaffold Induces Short-term Nerve Regeneration and Functional Recovery Following Sciatic Nerve Transection in Rats, Neuroscience 396 (2019) 94–107.
[20] M. Dominici, K.Le Blanc, I. Mueller, I. Slaper-Cortenbach, F. Marini, D. Krause, R. Deans, A. Keating, D. Prockop, E. Horwitz, Minimal criteria for defining multipotent mesenchymal stromal cells. The International Society for Cellular Therapy position statement, Cytotherapy 8 (4) (2006) 315–317.
[21] N. Maurmann, D.P. Pereira, D. Burguez, F.D.A.D.S. Pereira, P.I. Neto, R. A. Rezende, D. Gamba, J.V.L. Da Silva, P. Pranke, Mesenchymal stem cells cultivated on scaffolds formed by 3D printed PCL matrices, coated with PLGA electrospun nanofibers for use in tissue engineering, Biomed. Phys. Eng. Express. 3 (2017), https://doi.org/10.1088/2057-1976/aa6308.
[22] R.L. Siqueira, N. Maurmann, D. Burguêz, D.P. Pereira, A.N.S. Rastelli, O. Peitl, P. Pranke, E.D. Zanotto, Bioactive gel-glasses with distinctly different compositions: bioactivity, viability of stem cells and antibiofilm effect against Streptococcus mutans, Mater. Sci. Eng. C. (2017) 76, https://doi.org/10.1016/j.msec.2017.03.056.
[23] P.M. Dietrich, S. Glamsch, C. Ehlert, A. Lippitz, N. Kulak, W.E.S. Unger, Appl. Surf. Sci. 363 (2016) 406.
[24] J.F. Moulder, W.F. Stickle, P.E. Sobol, K.D. Bomben, Handbook of X-Ray Photoelectron Spectroscopy, J. Chastain and R. C. King (Eds.), Physical Electronics, US, 1995.
[25] A. Franquet, Characterization of Silane Films On Aluminium, PhD. Thesis in Departamento f Metallurgie Electrochemistry and Materials Science, Vrije Universiteit Brussel, Brussells, 2002.
[26] M.T. Kim, Deposition kinetics of silicon dioxide from tetraethylorthosilicate by PECVD, Thin Solid Films, v 360 (2000) 60–68.
[27] W. Han, F. Zhao, X. Yang, X. Shi, A mesoporous titanium glycolate with exceptional adsorption capacity to remove multiple heavy metal ions in water, RSC Adv. 7 (48) (2017) 30199–30204, v.
[28] C. Sharan, P. Poddar, P. Khandelwal, The mechanistic insight into the biomilling of goethite (α-FeO(OH)) nanorods using yeast saccharomyces cerevisiae, RSC Adv. 5 (111) (2015) 91785, v.
[29] Y.K. Lee, C.W. Chung, Ionization in inductively coupled argon plasmas studied by optical emission spectroscopy, J. Appl. Phys. 109 (2011), 013306 v.
[30] M.T. Kim, Deposition kinetics of silicon dioxide from tetraethylorthosilicate by PECVD, Thin Solid Films 360 (2000) 60–68.
[31] T.H. Chung, M.S. Kang, C.J. Chung, Y. Kim, Effects of process parameters on the properties of silicon oxide films using plasma enhanced chemical vapor deposition with tetramethoxysilane, Curr. Appl Phys. 9 (3) (2009) 598–604, v.
[32] M.T. Kim, Deposition kinetics of silicon dioxide from tetraethylorthosilicate by PECVD, Thin Solid Films 360 (2000) 60–68, v.

[33] J. Schäfer, J. Hnilica, J. Sperka, A. Quade, V. Kudrle, R. Foest, J. Voák, L. Zajicková, Tetrakis (trimmethylsilyloxy)silane for nanostructured $SiO_2$-like films deposited by PECVD at atmospheric pressure, Surf. Coat. Technol. 295 (2016) 112–118, v.
[34] O. Bazaka, K. Bazaka, V.K. Truong, I. Levchenko, M.V. Jacob, Y. Estrin, R. Lapovok, B. Chichkov, E. Fadeeva, P. Kingshott, R.J. Crawford, E.P. Ivanova, Effect of titanium surface topography on plasma deposition of antibacterial polymer coatings, Appl. Surf. Sci. 521 (146375) (2020) 1–16.
[35] I. Levchenko, M. Korobov, M. Romanov, M. Keidar, Ion current distribution on a substrate during nanostructure formation, J. Phys. D Appl. Phys. 37 (2004) 1690–1695.
[36] Z.L. Tsakadze, I. Levchenko, K. Ostrikov, S. Xu, Plasma-assisted self-organized growth of uniform carbon nanocone arrays, Carbon N Y 45 (2007) 2022–2030.
[37] S. Attarilar, M.T. Salehi, K.J.A. Fadhalah, F. Djavanroodi, M. Mozafari, Functionally graded titanium implants: characteristic enhancement induced by combined severe plastic deformation, PLoS One 14 (8) (2019) 1–18, v.
[38] L.M. Antonini, V. Kothe, G. Reilly, R. Owen, J.S. Marcuzzo, C.F. Malfatti, Effect of Ti6Al4V surface morphology on the osteogenic differentiation of human embryonic stem cells, J. Mater. Res. 32 (2017) 3811–3821, v.
[39] R. Ortiz, I. A.-Rodríguez, M. Rommel, I. Quintana, M. Vivanco, J.L.T. Herrera, Laser surface microstructuring of a bio-resorbable Polymer to anchor stem cells, control adipocyte morphology, and promote osteogenesis, Polymers (Basel) 12 (10) (2018) 1337, v.
[40] M. Bao, J. Xie, W.T.S. Huck, Recent advances in engineering the stem cell microniche in 3D, Adv. Sci. 5 (2018), 1800448 v.
[41] S. Attarilar, D. Faramarz, E. Mahmoud, A. Khaled, W. Liqiang, M. Masoud, Hierarchical microstructure tailoring of pure titanium for enhancing cellular response at tissue-implant interface, J. Biomed. Nanotechnol. 17 (1) (2021) 115–130, v.
[42] Q. Wang, P. Zhou, S. Liu, S. Attarilar, R.L.W. Ma, Y. Zhong, L. Wang, Multi-scale surface treatments of titanium implants for rapid osseointegration: a review, Nanomaterials 10 (1244) (2020) 1–27, v.
[43] S. Hwang, H. Seo, D.-.C. Jeong, L. Wen, Growth kinetics of plasma-polymerized films, Sci. Rep. 11201 (5) (2015) v.
[44] H. Rebl, B. Finke, R. Lange, K.-.D. Weltmann, J.B. Nebe, Impacto f plasma chemictry versus titanium surface topography on osteoblast orientation, Acta Biomater. 8 (2012) 3840–3851, v.
[45] F. Lüthen, R. Lange, P. Becker, J. Rychly, U. Beck, J.B. Nebe, The influence of surface roughness of titanium on beta1- and beta3-integrin adhesion and the organization of fibronectin in human osteoblastic cells, Biomaterials 26 (15) (2005) 2423–2440.
[46] K. Anselme, M. Bigerelle, B. Noël, A. Iost, P. Hardouin, Effect of grooved titanium substratum on human osteoblastic cell growth, J. Biomed. Mater. Res. 60 (4) (2002) 529–540.
[47] R. Lange, et al., Titanium surfaces structured with regular geometry – material investigations and cell morphology, Surf. Interface Anal. 42 (6–7) (2010) 497–501.